FFT-based coding algorithm with accurate rate control for space-borne SAR complex images

LI Ling[1,2], **WANG Zhen-song**[1]

1. *Institute of Computing Technology, Chinese Academy of Sciences, Beijing* 100190, *China*;
2. *Graduate University of Chinese Academy of Sciences, Beijing* 100049, *China*

Abstract: With the rapid development of SAR missions, on-board SAR image processing is required. SAR could obtain much higher resolution images than ordinary radar, and it is very necessary to compress data before transmission, since the generated SAR data volume is much higher than the data bandwidth of the satellite downlink. In this paper, an efficient compression algorithm with accurate rate control is proposed based on SAR complex image characteristics. The algorithm applies an adaptive weighted quantizer on 2D-FFT coefficients, and then uses entropy encoder to code the quantized coefficients. Based on the established R-Q and MPE-Q statistical models, an accurate rate control is developed. We measure the compression performance with PSNR and MSSIM (Mean Structural Similarity) of the magnitude image and MPE (Mean Phase Error). With four SAR complex images compressed at different ratios, the compression performance is analyzed and compared with other algorithms including JPEG2000, H.264, etc. Experimental results show that the proposed algorithm outperforms other algorithms, and the rate control obtains high accuracy.

Key words: space-borne SAR complex image, rate control, image compression

CLC number: TP732.1 **Document code:** A

1 INTRODUCTION

Space-borne Synthetic Aperture Radars (SAR) are active microwave imaging systems, and provide high resolution two-dimensional terrain imageries regardless of weather conditions. Radar systems are widely used in military reconnaissance, civil field, exploitation of natural resources, topography mapping, disaster monitoring (Curlander & McDonough, 1991; Guo *et al.*, 2007).

Early SAR systems transmit the raw echo data to ground stations, and then carry out image processing. With the development of VLSI and digital signal processing technology, it becomes possible to process space-borne SAR echo data on-board in real-time (Guo *et al.*, 2007). On-board SAR real-time imaging could observe the unexpected events in real-time, as well as identify and select the regions of interest of SAR image in real-time and abandon useless image blocks. SAR image compression can significantly reduce data storage and data transmission, lighten the burden of satellite download link, and reduce the download time (Guo *et al.*, 2007). Besides, it is possible to achieve higher compression ratios for SAR complex images, since the pixel correlation of the SAR complex image is higher than that of the raw echo data.

With the improvement of SAR resolution and mapping bandwidth, complex image data volume is increasing. For example, if the PRF (Pulse Repetition Frequency) of a radar satellite is 2000Hz, a 64K×16K image of 16-bit IQ channel produces a data rate of 4Gb/s. At present, the bandwidth of data-transmission system is generally 100—150Mb/s, and is much lower than the required data bandwidth. Therefore, it is necessary to study the efficient SAR complex image compression algorithm.

Compared to optical images, SAR images consist of 32-bit complex pixels with large dimensions, possess very high dynamic range, and exhibit very little spatial correlation (Eichel & Ives, 1999). Phase information of such images is necessary for SAR image applications, such as digital elevation. So far, more works focus on the compression of SAR magnitude images. And few researches concentrate on the SAR complex image compression.

Based on the processing methods of real and imaginary parts of SAR images, SAR image compression algorithms can be classified as three categories: independent compression of the two parts, compressing the two parts together, and independent compression of the magnitude and phase components. The first category of methods compresses the real and imaginary parts independently, such as the real-valued wavelet coding method (Ives *et al.*, 1998). They could not preserve the phase information effectively. The second category of methods is mainly

Received: 2008-11-17; **Accepted**: 2009-03-17

Foundation: 863 Program of China (No. 2006AA701119, 2006AA701415).

First author biography: Li Ling (1982—), female, Ph.D. student from the Institute of Computing Technology, Chinese Academy of Sciences. Her research interests include image/video compression, high performance computing. E-mail: liling@ict.ac.cn

Corresponding author: WANG Zhen-song, E-mail: zswang@ict.ac.cn

FFT-based coding method (Eichel & Ives, 1999; Xia *et al.*, 2006; Sun & Li, 2006), as well as the complex-valued wavelet coding method (Ives *et al.*, 1998). They could preserve the phase information much better. The third category of methods compresses the magnitude and phase components independently. The magnitude image is generally compressed with the wavelet or wavelet-packet coding method (Brandfass *et al.*, 1997), and could obtain higher compression ratios compared to complex images. The phase information generally follows the uniform distribution and possesses little correlation (Brandfass *et al.*, 1997). And it is difficult to compress.

Although the second category method could achieve higher compression ratios and preserve better phase information, there are still disadvantages. Previous FFT-based coding algorithms generally remove the zero-padded region in Fourier domain by a windowing function or weighted function, and encode the quantized coefficients by arithmetic or Huffman coding. However, little coding gain could be achieved by entropy coding the coefficients directly, since the quantized coefficients generally follow random distribution. Besides, efficient and accurate rate control is generally ignored, and it is not fit for the constant bandwidth transmission. In addition, most of the previous methods target air-borne SAR images, which has higher signal noise ratio than space-borne SAR images. Such methods generally could not achieve good compression performance for space-borne SAR images with low signal-to-noise ratio and wide mapping bandwidth.

In this paper, the compression method is studied for the space-borne SAR complex image. This method processes the real and imaginary parts together. The complex image is divided into several fixed-size blocks, and then transformed with 2D-FFT. The transform coefficients are quantized by an adaptive weighted quantizer, and then entropy coded by the bit-plane encoder. The relationship between the coding bit rate R and the quantization step size Q, as well as the relationship between the Mean Phase Error (MPE) and Q, are established. Based on the statistical attributes, the quantization step size and the threshold of the weighted function are adaptively adjusted to reduce the phase and magnitude distortions. We use PSNR and MSSIM (Mean Structural Similarity) of the magnitude image and MPE as the quality metrics. Extensive experimental results show that the coding system outperforms other algorithms at the same bit rate, including JPEG2000, H.264, HD Photo, etc. And the rate control method achieves high accuracy with the bit rate error lower than 0.15%.

2 QUALITY METRICS

Quality metrics measure the performance of a compression system. Since the SAR complex images contain magnitude and phase information, the quality metrics are different from the optical images. The following metrics are used in this paper to measure the coding performance.

2.1 PSNR of the magnitude image

The magnitude image of the SAR complex image is similar with the optical image, and reflects the terrain imaginaries of SAR scanning area. PSNR is used to measure the distortion.

$$\mathrm{PSNR}=10\log_{10}\frac{U^2}{\frac{1}{N_1\times N_2}\sum_{i=1}^{N_1}\sum_{j=1}^{N_2}[x(i,j)-\bar{x}(i,j)]^2} \tag{1}$$

where, $x(i, j)$ and $\bar{x}(i,j)$ are the (i, j) pixel values of the magnitude of the original and reconstructed complex images. N_1 and N_2 represent the azimuth number and the range number of the data respectively. U is the maximal pixel value of the original image.

2.2 Mean Structural Similarity (MSSIM) of the magnitude image

MSSIM (Mean Structural Similarity) (Wang *et al.*, 2004) measures the compression quality by the distortion of the structural information. Since human visual perception is sensitive to the structural information, MSSIM can measure the image quality better than the traditional PSNR metrics, especially for different coding algorithms. In recent years, MSSIM is widely used in image and video quality evaluation.

MSSIM is used to measure the magnitude image quality of the reconstructed complex image. The SSIM index is the product of the luminance, contrast and structure comparison functions, and is defined as (Wang *et al.*, 2004)

$$\mathrm{SSIM}(\boldsymbol{x},\boldsymbol{y})=\frac{(2\mu_x\mu_y+C_1)(2\sigma_{xy}+C_2)}{(\mu_x^2+\mu_y^2+C_1)(\sigma_x^2+\sigma_y^2+C_2)} \tag{2}$$

where, $\boldsymbol{x}$ and $\boldsymbol{y}$ are two nonnegative image signals. The constants $C_1=(K_1L)^2$ and $C_2=(K_2L)^2$ are included to avoid instability when $\mu_x^2+\mu_y^2$ is very close to zero. L is the dynamic range of the pixel values. $K_1\ll 1$ and $K_2\ll 1$ are small constants. In this paper, we set $K_1=0.01$ and $K_2=0.03$ according to (Wang *et al.*, 2004). An 11×11 circular-symmetric Gaussian weighting function $\boldsymbol{w}=\{w_i\mid i=1,2,\cdots,n\}$ is used, with standard deviation of 1.5 samples, normalized to unit sum $\sum_{i=1}^{n}w_i=1$. x_i and y_i are the pixels at the local window. The estimates of the local luminance statistics μ_x and μ_y, the contrast information σ_x and σ_y, as well as structural information σ_{xy} are calculated as

$$\mu_x=\sum_{i=1}^{n}w_ix_i,\quad \sigma_x=\sqrt{\sum_{i=1}^{n}w_i(x_i-\mu_x)^2},$$

$$\sigma_{xy}=\sum_{i=1}^{n}w_i(x_i-\mu_x)\,(y_i-\mu_y)$$

SSIM index reflects the local structural similarity. To evalu-

ate the overall image quality, MSSIM is calculated as the mean SSIM index (Wang *et al.*, 2004).

$$\mathrm{MSSIM}(\boldsymbol{X},\boldsymbol{Y})=\frac{1}{K}\sum_{j=1}^{K}\mathrm{SSIM}(\boldsymbol{x}_j,\boldsymbol{y}_j) \tag{3}$$

where, $\boldsymbol{X}$ and $\boldsymbol{Y}$ are the original and reconstructed images. $\boldsymbol{x}_j$ and $\boldsymbol{y}_j$ are the image contents at the jth local window. And K is the number of local windows of the image.

2.3 Mean phase error (MPE)

MPE (Mean phase error) is used to measure the phase distortion, and is defined as

$$\mathrm{MPE}=\frac{1}{N_1\times N_2}\sum_{i=1}^{N_1}\sum_{j=1}^{N_2}\left|\phi_{ij}-\varphi_{ij}\right| \tag{4}$$

where, ϕ_{ij} and φ_{ij} are the phases of the original and reconstructed images respectively.

2.4 Bit rate error

Compression bit rate and bit rate error are often used to measure the compression performance as well. For SAR complex images with 32bits per pixel (bpp), the bit rate fluctuation is generally required to be lower than 0.5% if the compression bit rate is at 1—8 bpp. In this paper, we use R_{error} to measure the rate control accuracy.

$$R_{\mathrm{error}}=(R_{\mathrm{result}}-R_{\mathrm{target}})/R_{\mathrm{target}}$$

where, R_{target} and R_{result} are the target bit rate and the actual compression bit rate respectively.

3 COMPRESSION ALGORITHM

The proposed compression algorithm contains several processing modules, including 2D-FFT, weighted quantization, rate control and entropy encoding, as shown in Fig. 1.

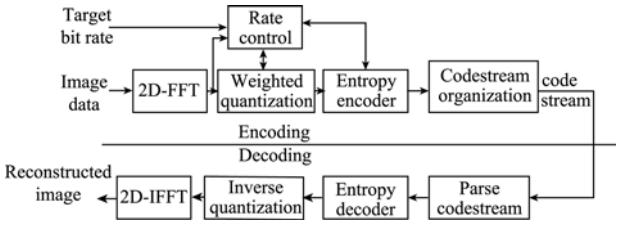

Fig. 1 Flowchart for encoding and decoding systems

3.1 Transform

After computing the 2D Fourier transform of a SAR complex image, there is a region of extremely small coefficients. This zero-padded region is added at the time of image formation to accomplish a specified image domain oversample ratio (Eichel & Ives, 1999). Fig. 2 shows the 128×128 magnitude images and the Fourier transform of complex images from BeijingArea (RADARSAT) and GoldstoneField (SEASAT). The zero-padded regions vary with image contents and satellites, but they represent 1/4 of the coefficients. This characteristic can be used to compress SAR complex images.

The transform block size would affect compression performance and the coding complexity. Larger block size could achieve higher compression performance, and increase the transform complexity. In this paper, the basic transform unit is composed of 128×128 pixels. The transformed data is quantized and entropy coded.

3.2 Weighted quantization

To remove the zero-padded region in Fourier domain, a weighted quantization is proposed. The weighted function is used to select non-zero coefficients which are quantized with the dead-zone scalar quantization. The weighted quantizer is defined as

$$y=\mathrm{Quan}(x)\times w(x)$$

where, x is the real or imaginary part of the transformed non-zero coefficients. $w(x)=\{\upsilon\,|\,\upsilon\in 0,1\}$ is a weighted function. $\mathrm{Quan}(x)=\mathrm{sign}(x)\lfloor|x|/Q\rfloor$ is a scalar quantization function. Q is the quantization step, and sign(x) is the sign of x. $|x|$ takes the absolute value of x, and $\lfloor|x|/Q\rfloor$ rounds down $|x|/Q$ to the nearest integer.

The choice of the weighted function depends on the data characteristic in frequency domain as well as the bits required to code the weighted values. Since the zero-padded regions are generally rectangular, it is much easier to encode the rectangular regions to reduce the bits required to encode the weighted values. Our proposed method takes a row or a column as the basic unit of zero-padded region, and calculates the sums of a row and a column to select the zero-padded region. Fig. 2 shows the magnitude images in frequency domain, and the distribution plots of the sums of a row and a column. Adaptively selecting appropriate row threshold T_{r} and column threshold T_{c} based on the frequency coefficients, could effectively discard the zero-padded region.

Denote the row sum and column sum with pixel x as $S_{\mathrm{r}}(x)$、$S_{\mathrm{c}}(x)$. The weighted function is defined as

$$w(x)=\begin{cases}1, & S_{\mathrm{r}}(x)\geqslant T_{\mathrm{r}}\ \ \&\ \ S_{\mathrm{c}}(x)\geqslant T_{\mathrm{c}}\\ 0, & \text{others}\end{cases}$$

The parameters Q, T_{r} and T_{c} affect the quantization and compressed bit rate. And they are determined by rate control, as illustrated in Section 3.4.

3.3 Entropy coding

Entropy coding is applied to the quantized coefficients to improve coding efficiency. Since the quantized real and imaginary parts generally follow random distribution, little coding gain could be obtained by directly applying arithmetic or Huffman coding. And the compression ratio is close to 1. From

Fig. 2, there are correlations among non-zero coefficients. The content adaptive embedded block encoder (Taubman, 2000; Taubman & Marcellin, 2002) can be applied to the quantized coefficients to improve the coding performance by utilizing the spatial redundancy.

The embedded block encoder scans the quantized coefficients by bit-plane, and determines the binary symbols to be encoded based on the sign and magnitude information of the neighbor samples. The binary symbols collected at bit plane coding are then encoded by an adaptive binary arithmetic encoder.

3.4 Rate control

As an important part of the compression system, rate control achieves optimal coding quality whilst meeting the target bit rate. We analyze the relationship between quantization step size (Q) and bit rate (R), as well as the relationship between the MPE and Q. Based on the established R-Q and MPE-Q models, an accurate rate control method is developed to determine the parameters of the quantization. The parameters include the threshold of the weighted function, and the quantization step size from the target bit rate and the encoded block information.

3.4.1 Threshold for weighted function

To remove the zero-padded region in frequency domain of the SAR complex image, a weighted function is applied. For different blocks, adaptively selecting the thresholds for row and column would improve the coding performance.

Experimental results show that for various blocks, $T_r=\max(S_r)\times T$ and $T_c=\max(S_c)\times T$. T is adaptively adjusted based on the bit rate of the current block. T approaches 0 at higher bit rate, equals 0.1 at middle bit rate, and is set to 0.2 otherwise. To reduce the errors caused by singular points, we set $\max(S_r)$ and $\max(S_c)$ as the mean values of the four maximal row sums and column sums, respectively.

3.4.2 Quantization step size

With the increasing demand for three-dimensional SAR image applications, it requires lower phase distortion and higher magnitude accuracy. Magnitude information is easier to compress than the phase information, and in practical systems the phase distortion is generally high when the magnitude distor-

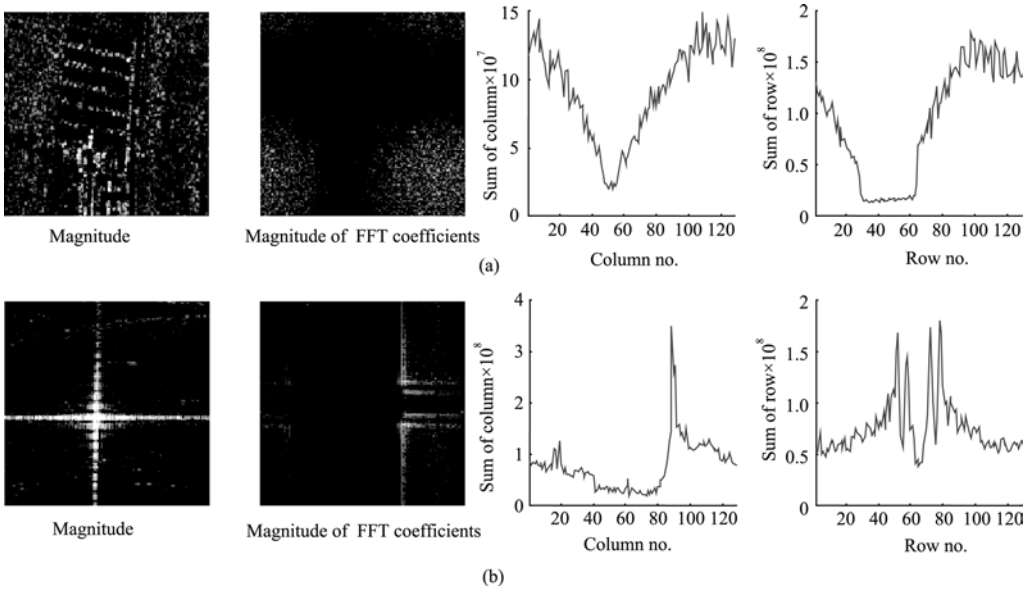

Fig. 2 Magnitude of original image and the FFT transformed image, distribution of the sum of row and sum of column.
(a) BeijingArea; (b) GoldstoneField

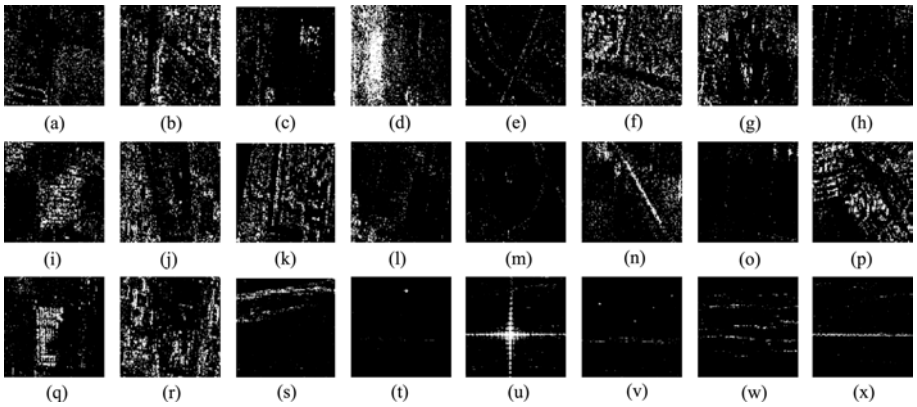

Fig. 3 Magnitude images of the tested complex image blocks

tion meets the target distortion. Therefore, to determine quantization step size, we give priority to the phase quality. In this subsection, the models of *R*-*Q* and MPE-*Q* are proposed, and the rate-distortion function is established to calculate the ideal quantization step size. In the following, the practical quantization step size determination is introduced.

To study the relationship of *R*-*Q*, as well as the relationship of MPE-*Q*, a set of SAR sample images of 128×128 sizes from different radar satellite and contents are selected as shown in Fig. 3. These images are compressed with the proposed compression method, and then the compression quality is evaluated. Fig. 4 and Fig. 5 show the *R*-*Q* and MPE-*Q* relationship of a part of the test blocks. For different blocks, *R* correlates logarithmically with *Q*, and MPE correlates linearly with *Q*. To establish the accurate *R*-*Q* and MPE-*Q* models, an image feature is selected as the model parameter. Since the statistical characteristics of the real and imaginary parts are similar, the mean absolute values of the real parts before transform is chosen as the image feature *M*. The expressions for *R*-*Q* and MPE-*Q* models are as follows

$$R = c\log_2(Q/M) + k \tag{5}$$

$$\mathrm{MPE} = aQ/M + b \tag{6}$$

c, *k* and *a*, *b* are the parameters of *R*-*Q* and MPE-*Q* models respectively.

The rate-distortion function minimizing MPE at a target bit rate for a complex image of *N* transform blocks is

$$\begin{cases} \min\left\{ f(\lambda) = \sum_i \mathrm{MPE}_i + \lambda \sum_i R_i \right\} \\ R = \sum_i R_i \Big/ N \leqslant R_{\mathrm{target}} \end{cases} \tag{7}$$

$$f(\lambda) = \sum_i \left(aQ_i/M_i + b\right) + \lambda \sum_i \left(c\log_2\left(Q_i/M_i\right) + k\right),\ \mathrm{MPE}_i,\ R_i,$$

Q_i and M_i are the MPE, bite rate, quantization step size and image feature for the *i*th image block. λ is the Lagrange multiplier. R_{target} and R are the target bit rate and the actual bit rate.

Solving (7), we get

$$\frac{\partial \mathrm{MPE}_i}{\partial R_i} = \frac{a\ln 2/M_i}{c/Q_i} = \frac{a\ln 2}{c}\frac{Q_i}{M_i} = -\lambda \tag{8}$$

(5) and (8) yield

$$R_i = c\log_2\left(Q_i/M_i\right) + k = c\log_2\left(-c\lambda/a/\ln 2\right) + k \tag{9}$$

Inserting (9) in (7) yields

$$R = \sum_i R_i = Nc\log_2\left(-c\lambda/a/\ln 2\right) + Nk \leqslant NR_{\mathrm{target}} \tag{10}$$

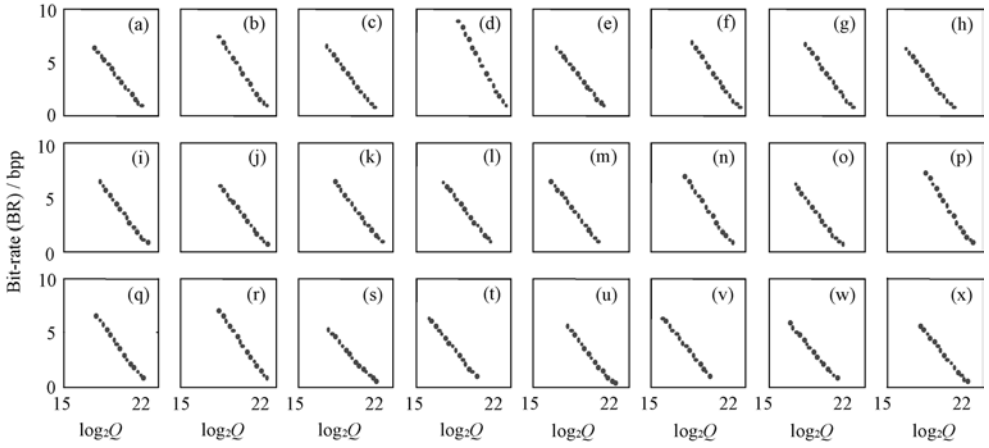

Fig. 4 The relation between BR and *Q*

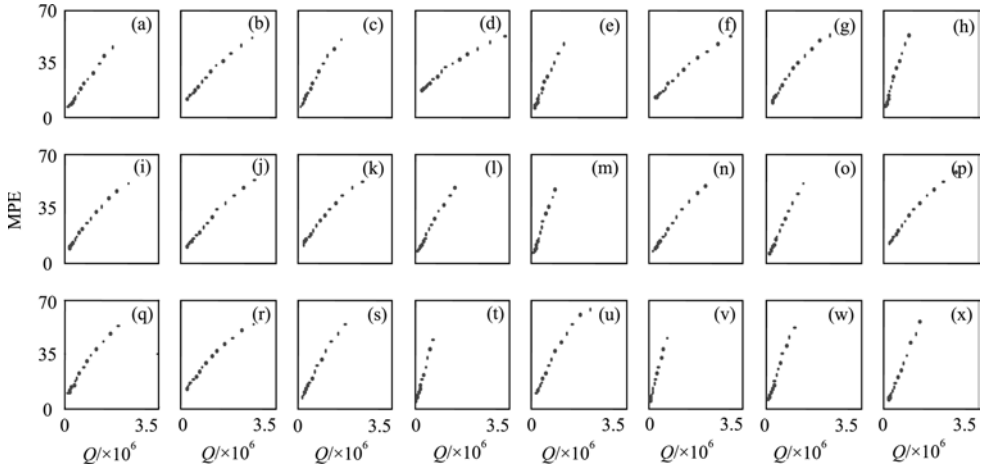

Fig. 5 The relation between MPE and *Q*

Solving (9) and (10) proves

$$Q_i = M_i 2^{\left(R_{\text{target}}-k\right)/c} \tag{11}$$

In the following, we obtain

$$\text{MPE}_i = aQ_i / M_i + b = a2^{\left(R_{\text{target}}-k\right)/c} + b \tag{12}$$

Therefore, the mean phase error MPE_i of each transform block equals to each other, and R_i is close to each other, and Q_i/M_i is similar.

From the above derivations, to minimize MPE, the bit rates of different blocks should be similar. If the parameters c and k can be obtained before compression by training, the quantization step size can be calculated from equation (11). Since the parameters c and k would be a little different for various images, there are estimation errors if Q is calculated with fixed c and k. In this paper, we use the linear regression method to calculate c and k for the current block with R-Q information of the encoded blocks. With the similarity between neighbor blocks, the estimation error is reduced compared to fixed c and k. The quantization step size Q_1 can be estimated with equation (5). To avoid Q_1 is too small or too large, we utilize the relationship between scalar quantization step size and bit rate (Taubman & Marcellin, 2002) to calculate $Q_2 = \left\lfloor \text{blkmax} / 2^{R_i} \right\rfloor$. Blkmax is the maximal absolute value of the real part in frequency domain. Q_1 is adjusted to the range of $\left[0.5\times Q_2, 2\times Q_2\right]$.

To determine the quantization step size, three procedures are included, such as quantization parameter initialization, quantization step size prediction and model parameter update. Fig. 6 illustrates the encoding flow with the quantization step decision module.

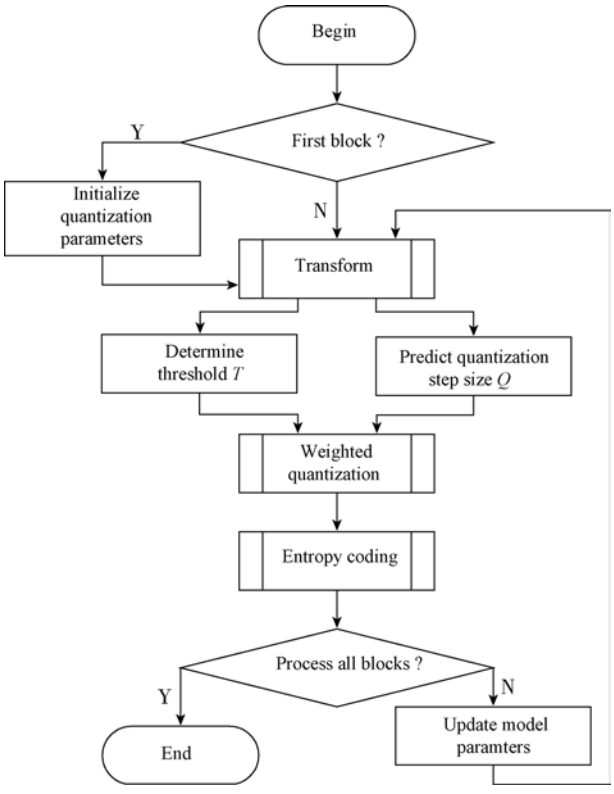

Fig. 6 Quantization step decision module vs. the coder

- Quantization parameter initialization: initialize the model parameters before quantizing the first block.
- Quantization step size prediction: predict Q_1 with the prediction model for current block, and calculate Q_2. Q_1 is adjusted with Q_2 to avoid the exceptional situations, and guarantees constant quality between neighbor blocks.
- Model parameter update: with the linear regression method, the parameters c and k are updated with the R and Q information of the encoded blocks.

4 EXPERIMENTAL RESULTS

The compression performance of the proposed method and the accuracy of rate control are analyzed in this section. And the coding performance is compared with different coding algorithms, including wavelet-based JPEG2000 (Taubman & Marcellin, 2002), lapped transform based HD Photo (Microsoft Corporation, 2006), integer block transform based H.264 (Wiegand *et al*., 2003), and wavelet packet based coding algorithm FWP (Meyer *et al*, 2000).

4.1 Test images

Four 4K×4K complex images are selected from RADARSAT and SEASAT. Fig. 7 shows the magnitude images of the test images. Each pixel has 16-bit signed integer real and imaginary parts (32bpp). Image BeijingArea is a scene of an urban area surrounding Beijing in north China. It contains many urban and natural features. Image GoldstoneField is a scene

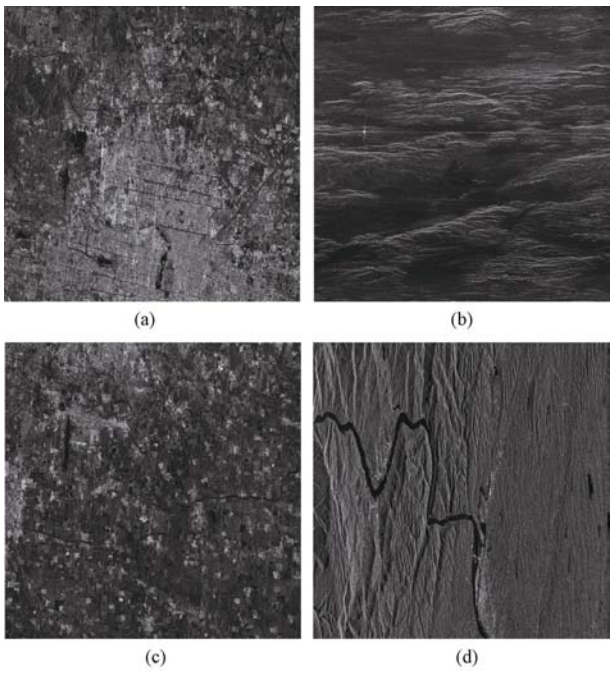

Fig. 7 The magnitude images of the tested complex images.
(a) BeijingArea; (b)GoldstoneField; (c)Field; (d)Sanxia

of the goldstone field from SEASAT containing several point targets on mountains. Image Field is a scene of rivers and fields with simple contents. Image Sanxia is the scene of the Three Gorges Dam region, and the ships in the image should be preserved.

4.2 Encoder parameters

Since the compared algorithms are real-valued method, we process the real and imaginary parts of the SAR complex images separately. An offset of 2^{15} is added so that the real and imaginary parts have an unsigned representation, and then they are compressed at the same bit rate.

Eichel and Ives (1999) analyzed the performance of the real-valued wavelets and complex wavelets. The real-valued wavelet outperforms the complex wavelet with the same quantization and entropy encoder. Therefore, we select the wavelet-based JPEG2000 as the representative encoder. Kakadu_v6.0 (Taubman, 2008) is used as the JPEG2000 encoder. 5 levels of 9/7 wavelet transform and 64×64 codeblock are used. The image is processed as one tile, and the quality layer information is not added to the COM segment. To obtain optimal coding performance, all bit planes are encoded and stored. Besides, the entropy encoder in this paper is similar to that of JPEG2000.

HD Photo (2006) is developed by Microsoft Corporation in 2007, and is under standardization as JPEG-XR. HD Photo applies the lapped transform with lower complexity than JPEG2000. And the coding performance is close to JPEG2000. HD Photo Device Kit v1.0 (2006) provided by Microsoft Corporation is used to compress images, in this paper. The test images are processed as the gray image of 16bpp with default parameters, and the quantization level is adjusted according to the target bit rate.

H.264 (Wiegand *et al.*, 2003) intra mode performs a variety of spatial predictions and integer transform of variable block sizes to improve the coding performance. The reference software JM13.2 is used, and High 10 Intra profile is applied in our experiments. Since JM13.2 can only process images with dimensions lower than 4K×2.5K (Tourapis *et al.*, 2007), we divide the 4K×4K images into two parts of 4K×2K sizes. The bit rate is adjusted by quantization parameters (QPISlice). The coding parameters for JM13.2 are summarized in Table 1, and others are default.

Table 1 Coding parameters for JM13.2

ProfileIDC	110	RDPsliceWeightOnly	0
LevelIDC	51	YUVFormat	0 (4:0:0)
RDPictureDecision	1	BitDepthLuma	16
RDPictureIntra	1	YUVFormat	0
RDOptimization	1	EnableIPCM	1

The wavelet packet coding algorithm of Meyer (2000) is used with the encoder FWP. 5 levels of wavelet packet decomposition are applied, and the frequency resolution of higher frequency band is not restricted.

4.3 Coding performance

We use the quality metrics introduced in Section 2 to measure the coding performance, including PSNR of magnitude image, MSSIM of magnitude image, and MPE. The target bit rates are set to 1 to 8bpp. JPEG2000, FWP and the proposed method could achieve accurate rate control. But HD Photo and H.264 need to compress images with several quantization levels to get the compressed bit stream closer to the target bit rate.

Fig. 8 shows the coding performance of the five compression algorithms for SAR complex images. At 1—8bpp, the proposed algorithm outperforms other algorithms at PSNR and MSSIM of magnitude image as well as MPE, especially the last two quality metrics. For Image BeijingArea, these algorithms have comparable PSNR performance at different bit rates. The proposed method performs slightly better. The performance of H.264 fluctuates a lot, and HD Photo performs worse. The proposed method outperforms other methods obviously for other test images, and PSNR is at least 1.5dB higher than other methods for image Sanxia. The proposed method has better MSSIM performance than other ones for the four test images. At lower bit rates, the coding gain is about 0.05—0.1. At higher bit rates, the distortion of different methods is very little and MSSIM is close to 1. At the bit rate of 1bpp, the MPE values of the proposed method are at least 9° lower than those of other methods on average. With the bit rate increasing, the distortion of complex image decreases, and the MPE values are close to each other for different compression methods.

Table 2 summarizes the coding performance of the five compression algorithm at the bit rate of 2 and 4bpp. The four values within each table cell from top to bottom represent the actual bit rate, PSNR of magnitude (dB), MSSIM of magnitude and MPE (°). The elements in bold indicate the optimal performance of the compression algorithms at the same bit rate for the current image.

The proposed algorithm outperforms other methods for several aspects. Firstly, the adopted FFT transforms the real and imaginary parts as a whole, and reduces the phase distortion compared to the independent process of the two parts. For example, FWP chooses the optimal wavelet packet basis for real and imaginary parts, and introduces different quantization errors for the two parts. Thus, it results in higher phase distortion. Secondly, a weighted quantization is used in the proposed method, and it can remove the redundancy in frequency domain. And the bit plane encoder can reduce the spatial redundancy of the transform coefficients. Finally, the proposed rate control

method minimizes the phase distortion at the target bit rate.

As shown in Fig. 8, there is an inflexion at 5—6bpp on the bit rate-PSNR curve of the proposed method. The inflexion is introduced by the selection of the threshold T for the weighted function. At the bit rate of 5—6bpp, MPE is lower and MSSIM is higher with higher threshold T, but PSNR is lower. At these bit rates, the PSNR value of the magnitude image are generally higher than 30dB, and the visual distortion is unobvious. Besides, MSSIM reflects the structural distortion better than PSNR. To obtain lower phase distortion and higher MSSIM, we choose 5bpp to be the cut-off point. Therefore, there is an inflexion at 5—6bpp.

Table 3 illustrates the bit rate error for different images at various bit rates, and the error unit is 10^{-3}. At different target bit rates, the bit rate error of the proposed method is lower than 10^{-3}. The only exception is -1.2442×10^{-3} for Sanxia image at 3bpp. And this bit rate error meets the accurate rate control requirement.

5 CONCLUSION

This paper analyzes the necessary of space-borne SAR complex image compression and the related works. Based on the characteristics, a FFT-based coding method is proposed. The complex image is divided into blocks, and then applies 2D-FFT. The transform coefficients are quantized with a weighted quantization, and then encoded by the bit-plane encoder. The R-Q and MPE-Q models are established for SAR complex images, and an accurate rate control is developed. Experimental results show that, the proposed method could achieve accurate rate control, and the bit rate error is lower than 0.15%. And it outperforms other methods at PSNR and MSSIM of magnitude as well as MPE.

The proposed method could meet the performance requirement for space-borne SAR complex images. Since the satellite processing system is restricted by the size, weight, limited computing power and so on, we would optimize the compression method, and implement it in real time.

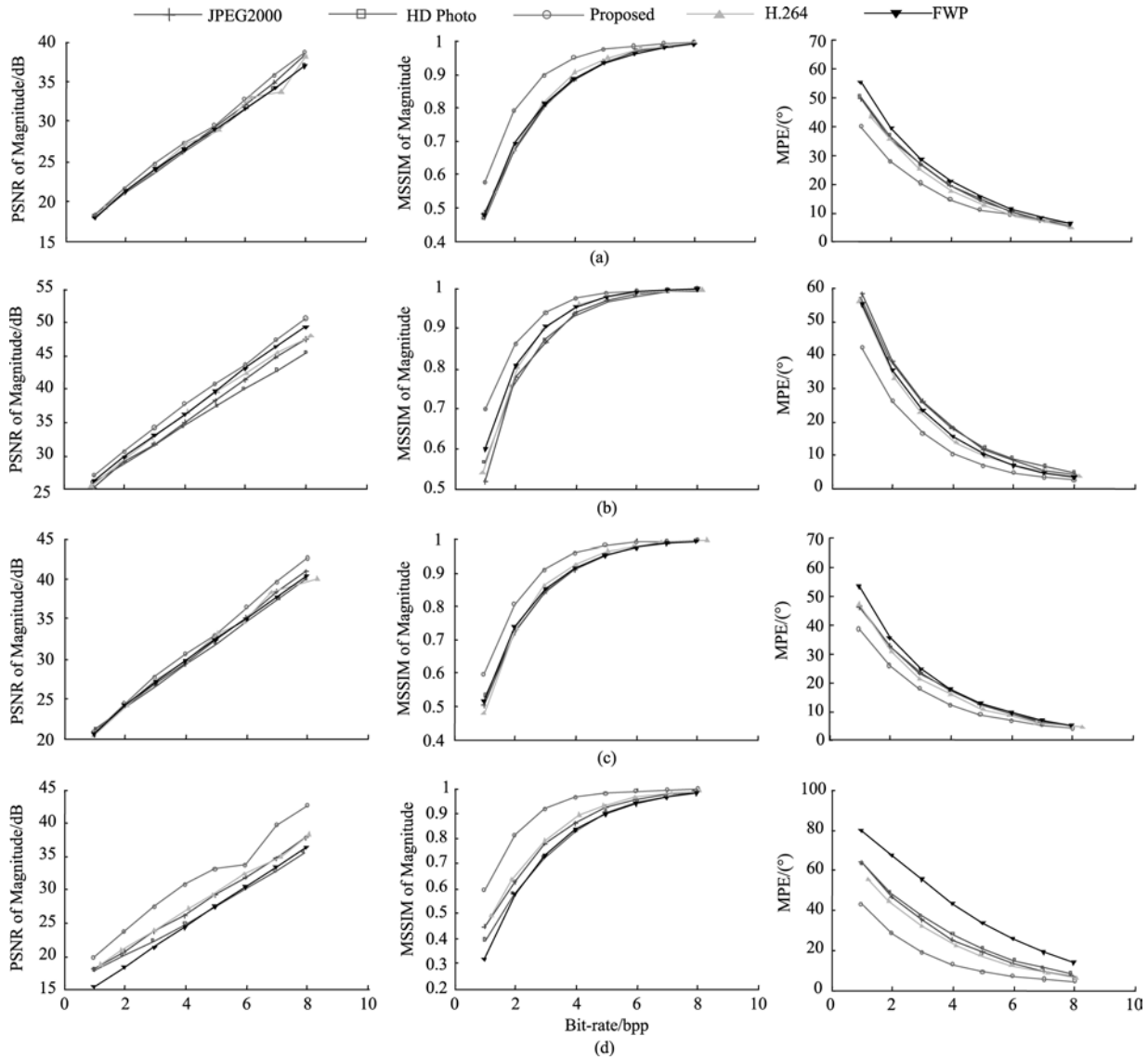

Fig. 8 Coding performance comparison
(a) Beijing Area; (b) Goldstone Field; (c) Field; (d) Sanxia

Table 2 Coding performance comparison for different coding algorithms at 2bpp and 4bpp

Test images	Target bit rate/bpp	JPEG 2000	HD Photo	H.264	FWP	Proposed
BeijingArea	4	4.0000	3.9254	4.0144	4.0000	3.9998
		26.5220	25.9383	27.1655	26.5375	**27.3686**
		0.8845	0.8801	0.9048	0.8863	**0.9481**
		22.1757	22.7649	19.8681	23.9125	**16.6652**
	2	1.9998	1.9690	1.9589	2.0000	1.9999
		21.2126	20.9275	21.1827	21.2910	**21.6273**
		0.6723	0.6700	0.6742	0.6930	**0.7898**
		40.9120	41.7184	40.4629	45.2728	**32.0314**
GoldstoneField	4	3.9998	3.9392	4.1102	4.0000	3.9997
		34.9795	34.2215	36.5373	36.2442	**37.7720**
		0.9379	0.9306	0.9594	0.9541	**0.9748**
		17.9315	18.0992	13.6294	15.3449	**10.2871**
	2	1.9999	1.9273	2.0615	2.0000	1.9998
		29.1735	28.5709	29.6163	29.7527	**30.4963**
		0.7793	0.7543	0.8041	0.8078	**0.8604**
		38.0230	38.6438	32.8946	35.4749	**26.1632**
Field	4	3.9998	3.9723	4.0079	4.0000	3.9996
		29.3970	29.1742	29.6360	29.7511	**30.6559**
		0.9069	0.9093	0.9235	0.9153	**0.9567**
		19.9296	19.2765	17.5143	20.1396	**13.7352**
	2	1.9998	2.0329	2.0570	2.0000	1.9998
		24.0458	24.0386	24.1585	24.2130	**24.4161**
		0.7231	0.7269	0.7340	0.7387	**0.8044**
		37.1796	36.5314	35.2944	40.7004	**29.4824**
Sanxia	4	3.9998	4.0008	4.1288	4.0000	3.9999
		25.9627	24.7181	27.1008	24.3270	**30.7386**
		0.8618	0.8317	0.8937	0.8351	**0.9636**
		25.3257	28.0754	21.9809	43.6849	**12.8827**
	2	1.9999	1.9659	1.8932	1.9999	2.0000
		20.7727	20.0529	20.8251	18.4296	**23.6654**
		0.6304	0.5803	0.6361	0.5776	**0.8157**
		46.7709	48.5385	44.4519	67.3649	**28.5368**

Table 3 The bit-rate error for different images and target bit-rates. The unit for bit-rate error is 10^{-3}

Target bit rate/bpp	BeijingArea	GoldstoneField	Field	Sanxia
1	–0.0787	0.1584	0.6580	0.4075
2	–0.0819	–0.0108	0.7965	0.1671
3	–0.0714	0.0025	0.6765	–1.2442
4	–0.0428	0.0131	–0.0232	–0.0219
5	–0.0451	–0.0750	0.1079	–0.0153
6	–0.0327	0.0361	–0.0483	–0.0172
7	–0.0296	–0.1116	–0.0858	–0.0083
8	0.0153	–0.2093	–0.0901	–0.0100

REFERENCES

Brandfass M, Coster W, Benz U and Moreira A. 1997. Wavelet based approaches for efficient compression of complex SAR image data. IEEE International Geoscience and Remote Sensing, **4**: 2024—2027

Curlander J C and McDonough R N. 1991. Synthetic Aperture Radar, Systems and Signal Processing. New York: Wiley

Eichel P and Ives R W. 1999. Compression of complex-valued SAR images. *IEEE Transactions on Image Processing*, **8**(10): 1483—1487

Guo M, Jian F J, Zhang Q, Xu B, Wang Z S and Han C D. 2007. FPGA-based real-time imaging system for spaceborne SAR. *Journal of Computer Research and Development*, **44**(3): 497—502

Ives R W, Magotra N and Kiser C. 1998. Wavelet compression of complex SAR imagery using complex- and real-valued wavelets: a comparative study. Conference Record of the Thirty-Second Asilomar Conference on Signals, Systems & Computers, **2**: 1294—

1298

Meyer F G, Averbuch A Z and Stromberg J O. 2000. Fast adaptive wavelet packet image compression. *IEEE Transactions on Image Processing*, **9**(5): 792—800

Microsoft Corporation. 2006. HD Photo Photographic Still Image File Format - Device Porting Kit Specification. Version 1.0

Sun M and Li C S. 2006. An adaptively weighted method based approach for data compression of complex-valued SAR images in frequency domain. *Journal of Electronics & Information Technology*, **28**(1): 12—15

Taubman D. 2000. High performance scalable image compression with EBCOT. *IEEE Transactions on Image Processing*, **9**(7): 1158—1170

Taubman D S and Marcellin M W. 2002. JPEG2000 Image Compression Fundamentals, Standards and Practice. Norwell, MA: Kluwer

Taubman D S. 2008. Kakadu V6.0 Software. http://www.kakadusoftware.com

Tourapis A M, Leontaris A, Sühring K and Sullivan G. 2007. H.264/MPEG-4 AVC Reference Software Manual. JVT-X072, Ed. Geneva, CH

Wang Z, Bovik A C, Sheikh H R and Simoncelli E P. 2004. Image quality assessment: from error visibility to structural similarity. *IEEE Transactions on Image Processing*, **13**(4): 600—612

Wiegand T, Sullivan G J, Bjntegaard G and Luthra A. 2003. Overview of the H.264/AVC video coding standard. *IEEE Transactions on Circuits and Systems for Video Technology*, **13**(7): 560—576

Xia W P, Wang Z S and Han J Z. 2006. A real-time data compression algorithm for SAR complex images based on block adaptive quantization. *Journal of Image and Graphics*, **11**(8): 1097—1104

基于 FFT 的星载 SAR 复数图像压缩及其码率控制算法

李 玲[1,2], 王贞松[1]

1. 中国科学院 计算技术研究所, 北京 100190;
2.中国科学院 研究生院, 北京 100049

摘 要: 分析了成像后的星载 SAR 复数图像压缩的必要性及复数图像特点, 对已有压缩算法做了简单分析。在此基础上, 提出一种基于 FFT 变换和加权量化的星载 SAR 复数图像压缩算法, 同时建立了适合 SAR 复数图像压缩的码率控制模型, 提出一种精确码率控制方法。实验结果表明, 以幅值 PSNR 和平均结构相似度以及平均相位误差为性能指标, 提出的 SAR 复数图像压缩算法优于现有压缩算法(JPEG2000、H.264 等); 同时, 提出的码率控制算法能够实现精确码率控制。

关键词: 星载 SAR 复数图像, 码率控制, 图像压缩

中图分类号: TP732.1 文献标识码: A

1 引 言

星载合成孔径雷达(SAR)作为一种全天时、全天候的有源主动微波成像系统, 以其优越的二维高分辨率特性, 在地质、自然资源勘探与监测、地形测绘和灾害估计等领域中得到了日益广泛的应用(Curlander & McDonough, 1991; Guo 等, 2007)。

早期的 SAR 系统, 需将原始回波数据下传至地面站进行成像处理。随着 VLSI 和数字信号处理技术的发展, 星载 SAR 回波数据在轨实时处理已成为可能(Guo 等, 2007)。在轨 SAR 实时成像不仅可以实现对突发性事件的实时观测, 还可以实时识别和选取 SAR 图像中感兴趣区域, 舍弃无用的图像块; 而 SAR 图像压缩可大幅减少需要存储和传输的数据量, 减轻卫星下行数据链路的负荷, 减少数据下传时间(Guo 等, 2007)。此外, 成像后的 SAR 复数图像数据的相关性远高于原始回波数据, 压缩比能够得到大幅提高。

随着 SAR 分辨率的提高和测绘带宽的增大, 复数图像数据量也不断增加。以某雷达卫星为例, 其脉冲重复频率(pulse repetition frequency, PRF)为 2000Hz, 取一帧图像的方位向长度为 16K(即 16384)点, 距离向长度为 64K(即 65536)点, 则一幅 IQ 两路均为 16 比特的 64K×16K 的数据, 其产生的数据率约为 4Gb/s。目前数传系统的带宽一般为 100—150Mb/s, 远远小于数据传输的需求。因此, 研究有效的 SAR 复数图像压缩算法是非常必要的。

相对光学图像, SAR 复数图像包含 IQ 两路数据、数据动态范围大、且数据相关性低(Eichel & Ives, 1999)。图像中存在大量相干斑噪声和点目标, 导致 SAR 复数图像像元间相关性较低。近年来复数图像压缩相关的研究不多, 较多的研究关注于成像后幅值(模值)图像的压缩, 忽略了相位信息的保持, 而相位信息的丢失限制了 SAR 图像的应用, 如数字高程等。

依据虚实部处理方式不同, 现有的 SAR 复数图像压缩算法可大致分为 3 类: 虚实部独立压缩、虚实部一起压缩以及幅值和相位独立压缩。第一类算法对复数图像的实部和虚部独立压缩, 如基于实数小波的方法等(Ives 等, 1998), 其缺点在于无法有效保持相位信息; 第二类算法主要是基于 FFT 的方法(Eichel & Ives, 1999; Xia 等, 2006; Sun & Li, 2006), 也有基于复数小波的方法(Ives 等, 1998), 对虚实部同时进行压缩处理, 可以获得较好的相位保持; 第

收稿日期: 2008-11-17; 修订日期: 2009-03-17

基金项目: 863 计划资助项目(编号: 2006AA701119, 2006AA701415)。

第一作者简介: 李玲(1982—), 女, 中国科学院计算技术研究所博士研究生。主要研究方向为图像/视频压缩、高性能计算。E-mail: liling@ict.ac.cn。

通讯作者: 王贞松, E-mail: zswang@ict.ac.cn。

三类算法将幅值和相位分开处理，通常幅值采用基于小波或小波包的压缩算法(Brandfass 等, 1997)，可以获得较高的压缩比，而相位近似均匀分布且相关性较低(Brandfass 等, 1997)，目前还没有比较好的压缩方法。

第二类方法虽然能够在取得较高压缩比的同时很好地保持相位信息，但仍存在一些不足。以往基于 FFT 的压缩算法，通常在频域通过加窗或加权函数去除零值区域以减少待编码比特数，随后对量化后的非零区域做算术编码或哈夫曼编码。由于量化后的数据近似随机分布，直接对其做算术编码或哈夫曼编码并不能获得较大增益。另外，现有方法未涉及精确码率控制，不适合恒定带宽信道传输。此外，现有方法大多是针对机载 SAR 复数图像，而机载 SAR 复数图像的信噪比通常高于星载 SAR 复数图像。对于低信噪比、宽测绘带的星载 SAR 复数图像，这些方法通常不能获得较好的压缩效果。

针对以上问题，研究了成像后的星载 SAR 复数图像压缩算法，采用虚实部一起压缩的方法。

2　性能指标

设计一个压缩系统时，首先要考虑所要满足的性能指标。对于 SAR 复数图像，由于其由实部和虚部组成，包含相位和幅值信息，因此在衡量压缩质量时，与光学图像有所不同。我们主要考虑采用以下指标来衡量压缩性能。

2.1　幅值图像 PSNR

复数图像取模可得到幅值图像。幅值图像类似于光学图像，反映 SAR 扫描区域的地貌信息，可以用 PSNR 来衡量失真情况:

$$\mathrm{PSNR}=10\log_{10}\frac{U^2}{\dfrac{1}{N_1\times N_2}\sum_{i=1}^{N_1}\sum_{j=1}^{N_2}[x(i,j)-\bar{x}(i,j)]^2} \quad (1)$$

式中，$x(i,j)$和$\bar{x}(i,j)$为压缩前后复数图像的幅值图像在(i,j)点的像元值。N_1和N_2是方位向和距离向样本点数，U指压缩前幅值图像的最大像元值。

2.2　幅值图像的平均结构相似度(MSSIM)

平均结构相似度(mean structural similarity, MSSIM)(Wang 等, 2004)根据结构信息损失程度来衡量压缩质量。由于人眼视觉系统对图像的结构信息较为敏感，相对传统的 PSNR 指标，MSSIM 能更好地反映压缩质量，尤其是可以更好地衡量不同算法的压缩性能。近年来，在图像和视频质量评估方面应用较广。

本文采用 MSSIM 来衡量压缩重建复数图像的幅值图像质量。像元点的结构相似度索引(SSIM index)定义为亮度(luminance)、对比度(contrast)和结构度(structure)的比较函数的乘积。通过下式(Wang 等, 2004)计算:

$$\mathrm{SSIM}(\boldsymbol{x},\boldsymbol{y})=\frac{\left(2\mu_x\mu_y+C_1\right)\left(2\sigma_{xy}+C_2\right)}{\left(\mu_x^2+\mu_y^2+C_1\right)\left(\sigma_x^2+\sigma_y^2+C_2\right)} \quad (2)$$

式中，$\boldsymbol{x}$ 和 $\boldsymbol{y}$ 表示两个非负的图像信号，常量 $C_1=(K_1L)^2$ 和 $C_2=(K_2L)^2$ 是为了避免当 $\mu_x^2+\mu_y^2$ 接近 0 时式(2)的不稳定。L 是像元的动态范围。$K_1\ll 1$ 和 $K_2\ll 1$是较小的常量值，根据 Wang 等(2004)取 $K_1=0.01$，$K_2=0.03$。以当前像元为中心点取 11×11 大小的图像窗($\boldsymbol{x}$ 和 $\boldsymbol{y}$)，将其中像元点记为 x_i 和 y_i，利用周期对称高斯加权窗函数 $\boldsymbol{w}=\{w_i\mid i=1,2,\cdots,n\}$ 计算得到: 当前位置像元的亮度信息μ_x 和μ_y，当前位置像元的对比度信息σ_x 和σ_y，以及结构度信息σ_{xy}。加权窗函数 $\boldsymbol{w}$ 的标准差为 1.5，归一化为 $\sum_{i=1}^{n}w_i=1$。可得到:

$$\mu_x=\sum_{i=1}^{n}w_ix_i,\quad \sigma_x=\sqrt{\sum_{i=1}^{n}w_i\left(x_i-\mu_x\right)^2}$$

$$\sigma_{xy}=\sum_{i=1}^{n}w_i\left(x_i-\mu_x\right)\left(y_i-\mu_y\right)$$

像元点的 SSIM 值反映了局部结构相似度信息。为了衡量整幅图像的质量，取各像元的 SSIM 的均值作为图像整体失真 MSSIM(Wang 等, 2004)，即

$$\mathrm{MSSIM}(\boldsymbol{X},\boldsymbol{Y})=\frac{1}{K}\sum_{j=1}^{K}\mathrm{SSIM}(\boldsymbol{x}_j,\boldsymbol{y}_j) \quad (3)$$

$\boldsymbol{X}$ 和 $\boldsymbol{Y}$ 是原始图像和重建图像; $\boldsymbol{x}_j$ 和 $\boldsymbol{y}_j$ 是第 j 个图像窗内的图像内容; K 是图像窗的总个数。

2.3　平均相位误差

在相位信息上，本文采用平均相位误差(mean phase error, MPE)来衡量相位失真，其计算公式为:

$$\mathrm{MPE}=\frac{1}{N_1\times N_2}\sum_{i=1}^{N_1}\sum_{j=1}^{N_2}\left|\phi_{ij}-\varphi_{ij}\right| \quad (4)$$

式中，ϕ_{ij} 和φ_{ij} 是原始图像和重建图像在(i,j)点的相位值。

2.4　码率误差

除了上述 3 个指标，压缩码率和码率波动也是常用的压缩性能指标。对于虚实部各 16 比特的 SAR

复数图像，一般要求压缩码率在 1—8 比特/像元，码率波动范围在 0.5%以下。本文以下述公式来衡量码率控制误差 R_{error}:

$$R_{\text{error}} = (R_{\text{result}} - R_{\text{target}}) / R_{\text{target}}$$

式中, R_{target} 和 R_{result} 分别是目标码率和压缩得到的实际码率。

3 压缩算法

本文提出的压缩系统包含以下几个主要处理步骤: 2D-FFT 变换、加权量化、码率控制和熵编码，如图 1。

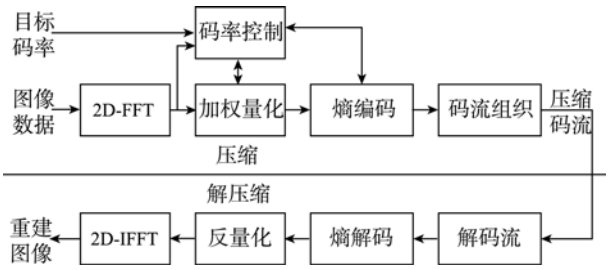

图 1 压缩和解压缩系统处理流程

3.1 变换

对于 SAR 复数图像, 2D-FFT 变换后的傅里叶系数存在连续的系数极小的区域，该区域内的系数接近零值，通常称为零值区域。这是由高分辨率 SAR 在频域过采样造成的(Eichel & Ives, 1999)。图 2 给出了从北京地区(BeijingArea, Radarsat)和金石场(GoldstoneField, Seasat)复数图像中提取出的 128×128 大小的复数图像块的幅值图像及其变换到频域后的幅值图像。不同卫星不同地域的复数图像，其零值区域不同；但零值区域通常会包含 1/4 以上的频域系数。利用频域冗余可有效压缩 SAR 复数图像。

变换块大小的选取影响压缩性能和压缩算法的复杂度。变换块较大时，通常可以获得较高的压缩性能，然而会增加变换的复杂度。本文选取 128×128 大小的变换块作为基本的变换单元，对变换后的数据块做量化和熵编码，最后对码流进行组织形成压缩文件。

3.2 加权量化

基于 2D-FFT 变换后频域数据存在零值区域的特点，提出加权量化策略。加权函数用于选取非零区域，非零区域采用死区标量量化 (dead-zone scalar quantization)。加权量化器如下:

$y = \text{Quan}(x) \times w(x)$, $\boldsymbol{x}$ 为变换后有效区域内的实部或虚部数据，Quan(x) 为标量量化函数，$w(x) = \{\upsilon \mid \upsilon \in 0,1\}$ 为加权函数。

Quan(x)定义为 $\text{Quan}(x) = \text{sign}(x)\left\lfloor |x| / Q \right\rfloor$, Q 为量化步长，sign(x)为取 x 的符号，$|x|$为取 x 的绝对值，$\left\lfloor |x| / Q \right\rfloor$ 为对$|x|/Q$ 向下取整。

加权函数的选取，需要综合考虑 SAR 复数图像数据的频域特点及权值编码所需的比特数。频域零值区域通常为规则的矩形区域，且矩形区域更易于编码以减少存储权值信息所需的比特数。因此在我们的算法中，把行或列作为基本的零值区域单元，

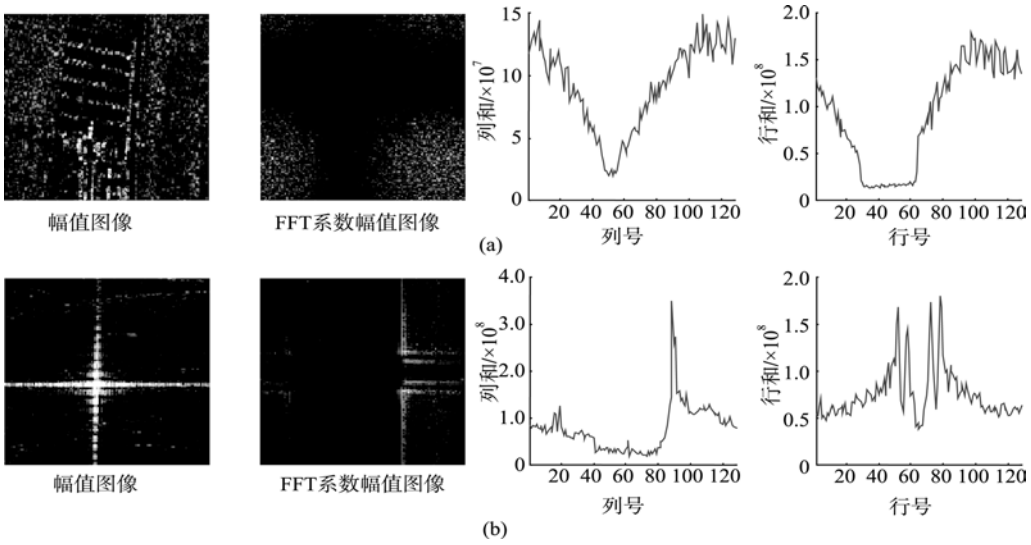

图 2 幅值图像、2D-FFT 后的幅值图像及其行和、列和分布

(a)北京地区图像; (b)金石场图像

计算行和、列和用于选择零值区域。图 2 给出了北京地区和金石场复数数据的频域幅值图，及行和、列和的分布图。根据频域系数自适应选择合适的行阈值 T_r 和列阈值 T_c，可以有效选取零值区域。

记像元点 x 所在频域数据的行和、列和分别为 $S_r(x)$、$S_c(x)$。加权函数可表示为:

$$w(x)=\begin{cases}1, & S_r(x)\geqslant T_r \ \ \& \ \ S_c(x)\geqslant T_c\\ 0, & \text{其他}\end{cases}$$

加权量化器中的参数 Q、T_r 和 T_c 对量化效果及结果压缩码率有直接影响，这些参数由码率控制算法确定，具体内容见 3.4 节。

3.3 熵编码

对量化后的非零区域的数据进行熵编码，以进一步提高压缩效率。量化后的实部和虚部数据近似随机分布，若直接对其做算术编码或哈夫曼编码，编码增益极低，所能获得的压缩比接近 1。从图 2 可以看出，非零区域数据存在一定的相似性，采用内容自适应的嵌入式块编码(Taubman, 2000; Taubman & Marcellin, 2002)对量化后的数据编码，可利用空间冗余性进一步提高压缩效率。

嵌入式块编码将量化后的数据按位平面扫描，根据块中已编码的邻近样本及块内其他样本的符号及幅值信息确定二进制符号的编码情况。位平面编码过程中收集到的二进制符号用自适应二进制算术编码做进一步编码。

3.4 码率控制

作为图像压缩系统的重要部分，码率控制的任务是在满足目标码率的同时，获得最优编码质量。针对 SAR 复数图像，分析了量化步长 Q 与码率 R 及平均相位误差 MPE 的关系；结合图像特征，建立了 R-Q 和 MPE-Q 模型；在此基础上，提出一种精确码率控制算法。该码率控制算法计算得到自适应加权量化所需的参数：确定加权量化权值函数的阈值，以及根据目标码率和已编码块信息确定当前块的量化步长。

3.4.1 加权函数阈值的确定

3.2 节介绍了 SAR 复数图像块的频域特点，频域数据中存在零值区域，利用加权函数确定该区域。为了获得良好的压缩效果，针对不同的数据块自适应选取行、列阈值。

对不同数据块的分析表明，当 $T_r=\max(S_r)\times T$ 且 $T_c=\max(S_c)\times T$ 时可获得较好的压缩效果。T 根据当前块的码率自适应调整：高码率时 T 趋于 0，中高码率时 T 设为 0.1，中低码率时 T 为 0.2 效果较优。为减少奇异点造成的选择误差，我们对 $\max(S_r)$和 $\max(S_c)$进行改进，以最大的 4 个行和、列和的均值进行替代。

3.4.2 量化步长的确定

随着对星载 SAR 三维图像需求的增加，要求相位误差更小、幅度定标更高。幅值相对相位较易压缩，在实际系统中当幅值满足质量要求时相位失真通常较大。因此在做量化步长选择时，优先考虑相位质量。

选取不同卫星和不同内容的 128×128 大小的复数图像块，如图 3，采用本文算法进行编码和质量评估。图 4、图 5 给出了一部分测试数据块的 R-Q 和 MPE-Q 曲线关系，可以看到压缩码率 R 和量化步长 Q 近似为对数关系，而 MPE 与量化步长近似为线性关系。不同的图像块均可用相同的函数形式来表示 R-Q 和 MPE-Q 关系，仅函数参数不同。为了准确地建立 R-Q 和 MPE-Q 关系模型，需要选取图像特征量作为模型参数。考虑到 SAR 复数图像的实部和虚部统计特征相似，本文取块数据变换前的实部的绝对平均值作为特征量 M，可以得到 R-Q 和 MPE-Q 模型的表达式为:

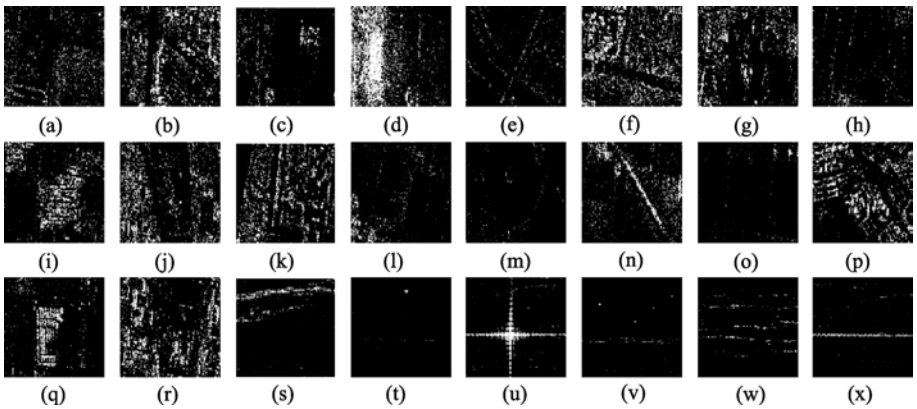

图 3 测试复数图像块的幅值图像

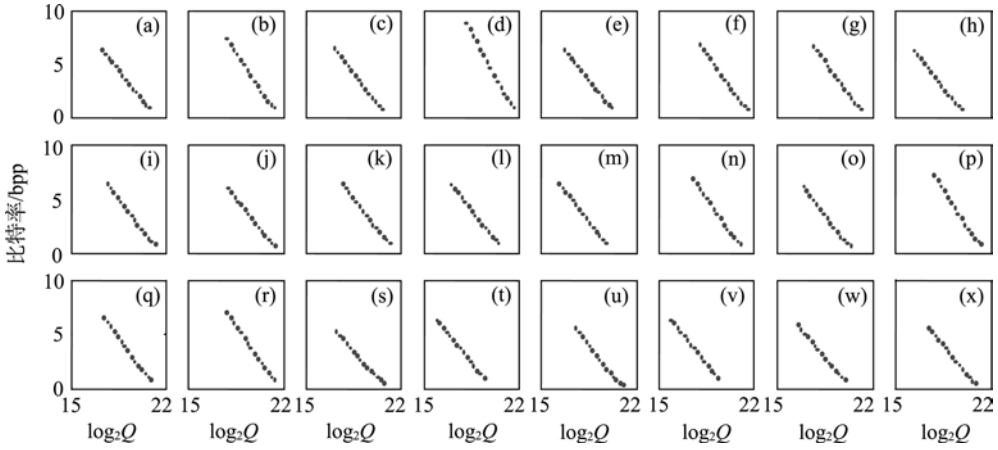

图 4 码率和量化步长关系

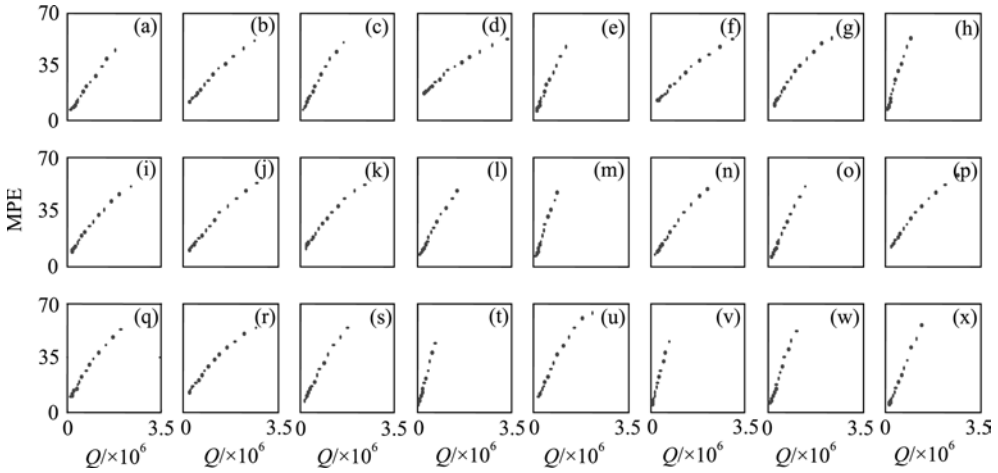

图 5 平均相位误差和量化步长关系

$$R = c\log_2\left(Q/M\right) + k \tag{5}$$

$$\mathrm{MPE} = aQ/M + b \tag{6}$$

c、k 和 a、b 分别为模型 R-Q 和 MPE-Q 的参数。

对于一幅包含 N 个变换块的复数图像，为了在目标码率下获得较低的平均相位失真，可建立率失真函数:

$$\begin{cases} \min\left\{ f(\lambda) = \sum_i \mathrm{MPE}_i + \lambda \sum_i R_i \right\} \\ R = \sum_i R_i \Big/ N \leqslant R_{\mathrm{target}} \end{cases} \tag{7}$$

$$f(\lambda) = \sum_i \left(aQ_i/M_i + b\right) + \lambda \sum_i \left[c\log_2\left(Q_i/M_i\right) + k\right],$$

MPE_i、R_i、Q_i 和 M_i 分别为第 i 个图像块的平均相位误差、码率、量化步长和特征量。λ为拉格朗日乘子，R_{target} 和 R 分别为复数图像压缩后的目标码率及实际码率。

根据拉格朗日极值法得到:

$$\frac{\partial \mathrm{MPE}_i}{\partial R_i} = \frac{a\ln 2/M_i}{c/Q_i} = \frac{a\ln 2}{c}\frac{Q_i}{M_i} = -\lambda \tag{8}$$

根据式(5)和式(8)得到:

$$R_i = c\log_2\left(Q_i/M_i\right) + k = c\log_2\left(-c\lambda/a/\ln 2\right) + k \tag{9}$$

将式(9)带入 R 的约束条件得到:

$$R = \sum_i R_i = Nc\log_2\left(-c\lambda/a/\ln 2\right) + Nk \leqslant NR_{\mathrm{target}} \tag{10}$$

解式(9)和式(10)得到: $Q_i = M_i 2^{\left(R_{\mathrm{target}} - k\right)/c}$ (11)

从而得到:

$$\mathrm{MPE}_i = aQ_i/M_i + b = a2^{\left(R_{\mathrm{target}} - k\right)/c} + b \tag{12}$$

即达到最优时，各变换块的 MPE_i 失真相同，且 R_i 近似相等，Q_i/M_i 近似相等。

从上述推导可以看出，为使 MPE 失真最小，只需满足各块的码率近似相等。若在压缩前通过训练获得 c、k 值，则可由式(11)计算得到各块的量化步长。考虑到实际数据的 c、k 值会随图像数据的不同而略有差异，若固定 c、k 值用式(11)计算各块的量

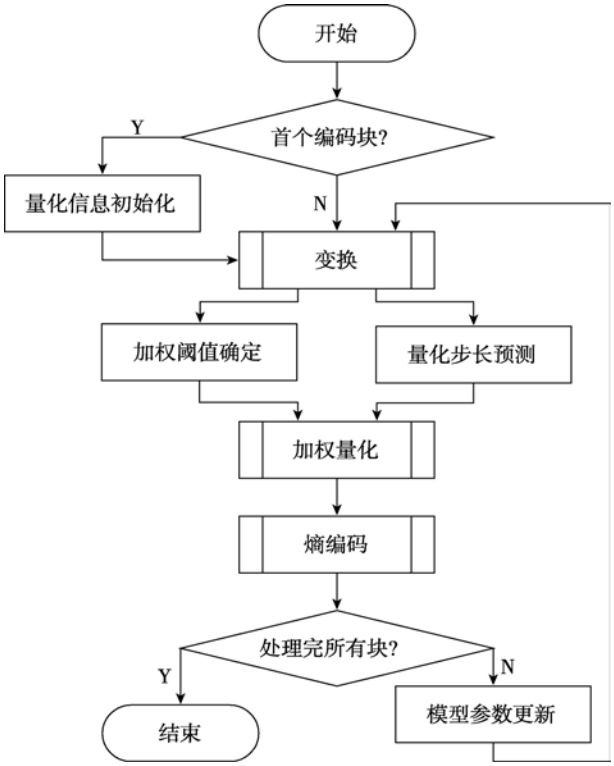

图 6　量化步长确定在编码器中所处的位置

化步长会存在一定的误差。采用线性回归方法，利用已编码块的 *R*-*Q* 信息估算当前编码图像块的 *c*、*k* 值。由于已编码块与当前块邻近，图像统计特性相似，采用该方法可减少因固定 *c*、*k* 值引入的误差。得到 *c*、*k* 值后可根据式(5)估算当前块的量化步长 Q_1。为了防止 Q_1 值过小或过大等例外情况，根据标量量化步长与码率的关系(Taubman & Marcellin, 2002)，计算得到量化步长 $Q_2=\left\lfloor \mathrm{blkmax}/2^{R_i} \right\rfloor$，blkmax 为当前块频域的实部的最大绝对值。根据 Q_2 对 Q_1 做进一步调整，使其取值范围在 $[0.5\times Q_2, 2\times Q_2]$ 内。

为了确定量化步长，需包含量化信息初始化、量化步长预测和模型参数更新 3 个计算步骤。图 6 给出了 3 个步骤在整个编码流程中所处的位置。

- 量化信息初始化：需要在图像的首个变换块量化前，初始化量化模型的参数。
- 量化步长预测：根据预测模型计算当前块的量化步长 Q_1，同时计算量化步长 Q_2；然后根据已编码数据块的量化步长和 Q_2 对 Q_1 进行调整，避免 Q_1 出现极小值或极大值等例外情况，同时使得相邻编码块质量较为稳定。
- 模型参数更新：通过线性回归方法，利用已编码数据的 *R*、*Q* 信息更新 *R*-*Q* 模型的参数 *c*、*k*。

4　算法性能分析

分析压缩算法性能及码率控制的准确度，并与基于不同变换、量化和熵编码的压缩算法做性能比较和分析。比较的算法包括：基于小波变换的 JPEG2000 算法(Taubman & Marcellin, 2002)、基于重叠变换的 HD Photo(Microsoft Corporation, 2006)、基于整数块变换的 H.264(Wiegand 等, 2003)以及基于小波包分解的 FWP 压缩算法(Meyer 等, 2000)。

4.1　测试图像

为了测试压缩算法对不同内容的复数图像的压缩性能，从 Radarsat 和 Seasat 卫星复数图像中选取 4 幅 4K×4K 大小的图像数据，其幅值图像如图 7。复数图像的实部和虚部均为 16 比特有符号数。北京地区图像内容为北京市区及周边信息，内容较为复杂；金石场图像为包含点目标(9 个角反射器)的山地图像，内容较为简单，但压缩时需有效保留点目标信息；田地(Field)图像为河流和分块的田地信息，内容较为简单；三峡(Sanxia)图像为三峡大坝地区场景，需有效保证江中船只信息。

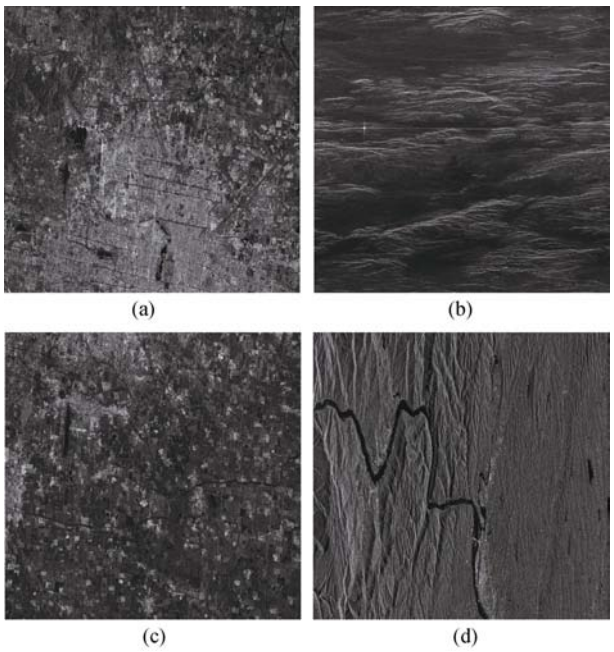

图 7　测试复数图像的幅值图像
(a)北京地区; (b)金石场; (c)田地; (d)三峡

4.2　编码器参数

由于待比较的算法均是实数域的，为了用于 SAR 复数图像压缩，将实部和虚部独立处理。首先将实部和虚部数据从有符号数加 2^{15} 变为无符号数，然后在相同的码率下分别压缩。

Eichel和Ives(1999)对实数小波和复数小波的性能分析表明，在相同量化和熵编码下，实数小波压缩性能优于复数小波压缩性能。为此，我们选择JPEG2000代表基于离散小波变换的压缩算法，参考软件为kakadu_v6.0(Taubman, 2008)。采用5级9/7小波和64×64大小的编码块，将整幅图像作为一个拼接块(tile)，禁止向注释标记段(COM)中添加质量层信息，同时对所有位平面进行编码和存储。本文算法采用的熵编码方法与JPEG2000熵编码算法基本一致。

2007年微软公司提出的HD Photo(2006)算法基于重叠块变换，复杂度低于JPEG2000，压缩质量与JPEG2000相近。本文采用微软公司提供的参考软件HD Photo Device Kit v1.0(2006)。测试图像作为每像元16比特的灰度图采用默认参数进行压缩，量化级数根据码率要求调整。

H.264(Wiegand 等, 2003)编码算法对帧内图像做基于空间相邻块的多种预测和块大小可变的整数变换以提高编码效率。采用high 10 Intra profile模式对数据进行压缩，参考软件为JM13.2。由于该参考软件不能处理分辨率大于4K×2.5K的图像(Tourapis等, 2007)，我们将图像分为4K×2K两块分别处理。将图像数据作为I-帧，通过改变量化参数(QPISlice)来调整码率。除了表1中的参数，其他编码参数采用默认值。

表 **1** **JM13.2** 编码参数

ProfileIDC	110	RDPsliceWeightOnly	0
LevelIDC	51	YUVFormat	0 (4:0:0)
RDPictureDecision	1	BitDepthLuma	16
RDPictureIntra	1	YUVFormat	0
RDOptimization	1	EnableIPCM	1

基于小波包的编码算法，我们采用Meyer(2000)的编码器FWP。编码采用5级包分解，同时不限制高频子带的频率分辨率。

4.3 压缩性能

我们采用第2部分提到的幅值PSNR、幅值MSSIM和平均相位误差MPE来衡量压缩性能，目标码率为1—8比特/像元。JPEG2000、FWP和本文算法均可以获得精确码率控制；而HD Photo和H.264不能获得精确率控，需要采用不同量化级数多次编码以获得接近目标码率的压缩码流。

图8依次给出了5种算法用于SAR复数图像压缩的性能。可以看出，在1—8比特/像元码率范围内，本文的算法在幅值PSNR、幅值MSSIM和MPE方面均优于其他算法。尤其在MSSIM和MPE性能指标下，对于不同的图像，本文的算法均显著优于其他算法。在幅值PSNR指标上，对于北京地区复数图像，几种算法性能差异不大，在不同码率下，本文算法略优于其他算法，H.264性能波动较大，HD Photo整体性能较低；对于其他几幅图像，本文算法明显优于其他几种算法，尤其对于三峡图像数据，PSNR值比其他算法高1.5dB以上。在幅值MSSIM指标上，对于4幅测试图像，相对其他算法，本文算法均有明显优势；中低码率下，本文算法增益约0.05—0.1；高码率下，几种算法失真均较低，该指标均趋于1。在MPE指标上，码率为1比特/像元时，本文算法平均相位失真比其他算法至少降低9°；随着码率的提高，复数图像失真减小，不同算法的平均相位失真趋于一致。

为了便于比较，表2给出了2比特/像元和4比特/像元下，不同算法对测试图像的压缩性能。每个单元格内的4个值从上到下依次表示压缩后码率、幅值PSNR(dB)、幅值MSSIM和平均相位误差MPE(°)。其中加黑的部分表示，对于当前图像在相同码率下几种算法的最佳性能。

本文提出的压缩算法之所以能够取得优于其他4种算法的压缩性能，一方面是由于FFT变换将实部和虚部作为整体进行变换，避免了虚实部分别处理引入的相位失真。如FWP对实部和虚部分别做最优小波包基选择，会造成实部和虚部量化误差不一致，引起较大的平均相位失真。另一方面，本文算法采用加权量化方法，有效地去除了频域冗余，同时又采用基于位平面的块编码方法，进一步去除了变换系数的空间冗余。最后，本文提出的码率控制算法，在率失真意义上，实现了相同码率下相位失真最小。

从图8可以看到本文算法的幅值PSNR在5—6比特/像元之间出现一个拐点。该拐点的产生是由FFT变换后频域数据的加权函数阈值 T 的选取造成的。在码率为5—6比特/像元范围内，阈值 T 越大，则重建图像的相位误差越小、MSSIM越高，但PSNR值变低。在该码率范围内，图像的PSNR值通常大于30dB，幅值图像视觉失真不明显；此外，MSSIM相对PSNR能更好地反映幅值图像的结构信息损失。为了保证较低的相位误差和较高的MSSIM，以5比特/像元作为加权阈值 T 选取的分界点，因此会在5—6比特/像元码率范围内出现一个拐点。

不同图像在不同码率下的码率误差如表 3 所示，表中误差值的单位是 10^{-3}。可以看出，在不同目标码率下，图 8 所示图像的码率误差基本低于 10^{-3}，仅在 3 比特/像元时，Sanxia 图像的码率误差为 -1.2442×10^{-3}。在此误差下，可认为满足精确码率控制的要求。

5　结论与讨论

本文首先分析了星载 SAR 复数图像压缩的必要性及现有压缩算法的不足。结合星载 SAR 复数图像特点，提出一种基于 FFT 的压缩算法。该算法对 2D-FFT 变换后的频率系数做加权量化，并采用基于位平面的块编码进一步提高压缩效率。本文同时建立了适用于 SAR 复数图像压缩的 *R-Q* 模型和 MPE-*Q* 模型，提出一种精确码率控制方法。实验结果表明，本文提出的算法能够实现精确码率控制，码率误差可以控制在 10^{-3} 数量级；并且在幅值 PSNR、幅值 MSSIM 和平均相位误差 MPE 上，也获得了优于其他算法的性能。

本文提出的算法可以满足星载 SAR 图像压缩性能要求。考虑到星上处理系统受体积、重量等限制，计算能力有限，将进一步优化压缩算法，并完成算法的实时化。

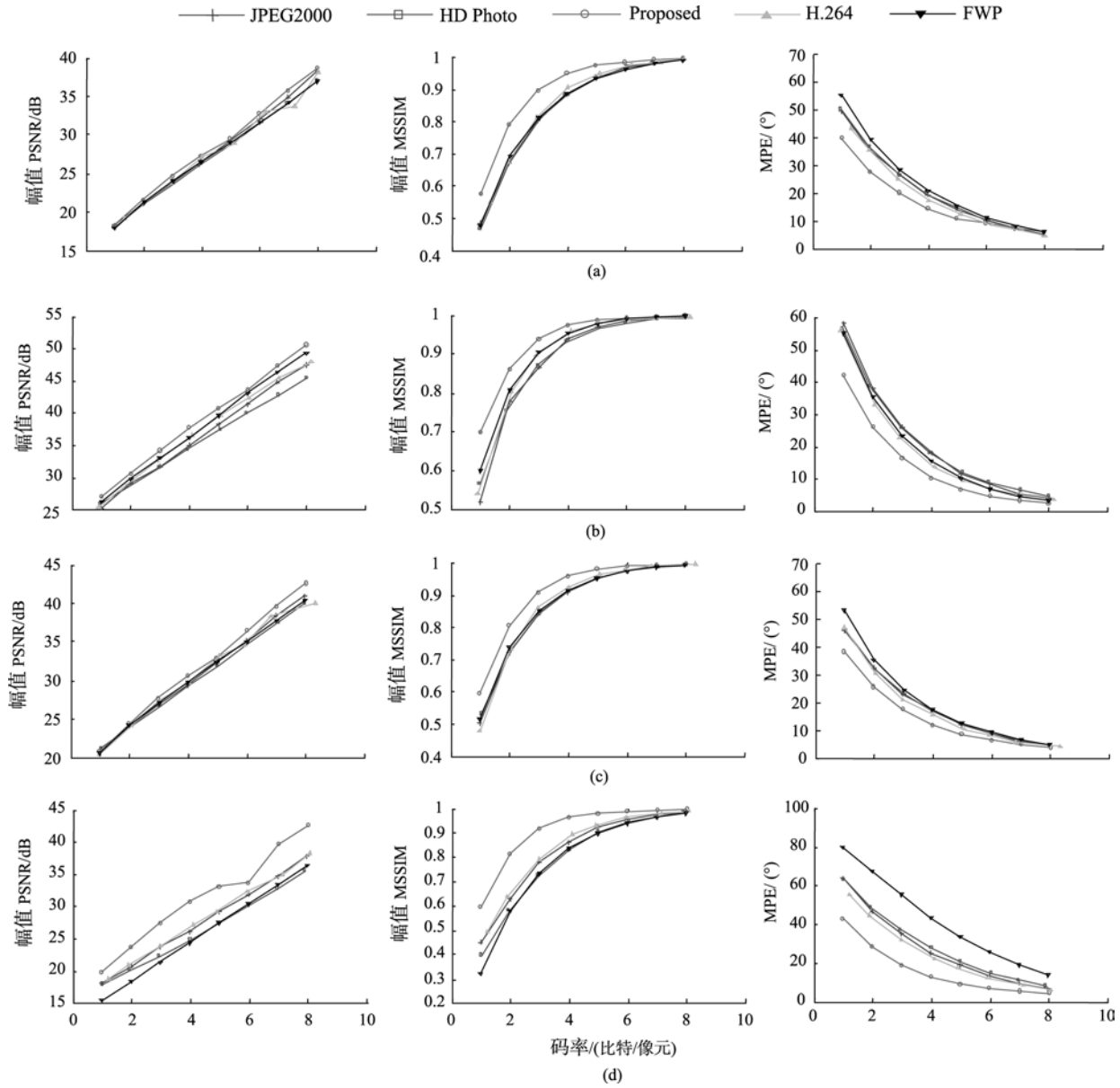

图 8　性能比较

(a)北京地区; (b)金石场地区; (c)田地; (d)三峡地区

表 2 目标码率 2 比特/像元和 4 比特/像元下，不同算法的压缩性能比较

测试图像	目标码率/(比特/像元)	JPEG 2000	HD Photo	H.264	FWP	Proposed
北京地区	4	4.0000	3.9254	4.0144	4.0000	3.9998
		26.5220	25.9383	27.1655	26.5375	**27.3686**
		0.8845	0.8801	0.9048	0.8863	**0.9481**
		22.1757	22.7649	19.8681	23.9125	**16.6652**
	2	1.9998	1.9690	1.9589	2.0000	1.9999
		21.2126	20.9275	21.1827	21.2910	**21.6273**
		0.6723	0.6700	0.6742	0.6930	**0.7898**
		40.9120	41.7184	40.4629	45.2728	**32.0314**
金石场	4	3.9998	3.9392	4.1102	4.0000	3.9997
		34.9795	34.2215	36.5373	36.2442	**37.7720**
		0.9379	0.9306	0.9594	0.9541	**0.9748**
		17.9315	18.0992	13.6294	15.3449	**10.2871**
	2	1.9999	1.9273	2.0615	2.0000	1.9998
		29.1735	28.5709	29.6163	29.7527	**30.4963**
		0.7793	0.7543	0.8041	0.8078	**0.8604**
		38.0230	38.6438	32.8946	35.4749	**26.1632**
田地	4	3.9998	3.9723	4.0079	4.0000	3.9996
		29.3970	29.1742	29.6360	29.7511	**30.6559**
		0.9069	0.9093	0.9235	0.9153	**0.9567**
		19.9296	19.2765	17.5143	20.1396	**13.7352**
	2	1.9998	2.0329	2.0570	2.0000	1.9998
		24.0458	24.0386	24.1585	24.2130	**24.4161**
		0.7231	0.7269	0.7340	0.7387	**0.8044**
		37.1796	36.5314	35.2944	40.7004	**29.4824**
三峡	4	3.9998	4.0008	4.1288	4.0000	3.9999
		25.9627	24.7181	27.1008	24.3270	**30.7386**
		0.8618	0.8317	0.8937	0.8351	**0.9636**
		25.3257	28.0754	21.9809	43.6849	**12.8827**
	2	1.9999	1.9659	1.8932	1.9999	2.0000
		20.7727	20.0529	20.8251	18.4296	**23.6654**
		0.6304	0.5803	0.6361	0.5776	**0.8157**
		46.7709	48.5385	44.4519	67.3649	**28.5368**

表 3 不同图像和码率下码率误差 $/10^{-3}$

目标码率/(比特/像元)	北京地区	金石场	田地	三峡
1	–0.0787	0.1584	0.6580	0.4075
2	–0.0819	–0.0108	0.7965	0.1671
3	–0.0714	0.0025	0.6765	–1.2442
4	–0.0428	0.0131	–0.0232	–0.0219
5	–0.0451	–0.0750	0.1079	–0.0153
6	–0.0327	0.0361	–0.0483	–0.0172
7	–0.0296	–0.1116	–0.0858	–0.0083
8	0.0153	–0.2093	–0.0901	–0.0100

REFERENCES

Brandfass M, Coster W, Benz U and Moreira A. 1997. Wavelet based approaches for efficient compression of complex SAR image data. IEEE International Geoscience and Remote Sensing, **4**: 2024—2027

Curlander J C and McDonough R N. 1991. Synthetic Aperture Radar, Systems and Signal Processing. New York: Wiley

Eichel P and Ives R W. 1999. Compression of complex-valued SAR images. *IEEE Transactions on Image Processing*, **8**(10): 1483—1487

Guo M, Jian F J, Zhang Q, Xu B, Wang Z S and Han C D. 2007. FPGA-based real-time imaging system for spaceborne SAR. *Journal of Computer Research and Development*, **44**(3): 497—502

Ives R W, Magotra N and Kiser C. 1998. Wavelet compression of complex SAR imagery using complex- and real-valued wavelets: a comparative study. Conference Record of the Thirty-Second Asilomar Conference on Signals, Systems & Computers, **2**: 1294—1298

Meyer F G, Averbuch A Z and Stromberg J O. 2000. Fast adaptive wavelet packet image compression. *IEEE Transactions on Image Processing*, **9**(5): 792—800

Microsoft Corporation. 2006. HD Photo Photographic Still Image File Format - Device Porting Kit Specification. Version 1.0

Sun M and Li C S. 2006. An adaptively weighted method based approach for data compression of complex-valued SAR images in frequency domain. *Journal of Electronics & Information Technology*, **28**(1): 12—15

Taubman D. 2000. High performance scalable image compression with EBCOT. *IEEE Transactions on Image Processing*, **9**(7): 1158—1170

Taubman D S and Marcellin M W. 2002. JPEG2000 Image Compression Fundamentals, Standards and Practice. Norwell, MA: Kluwer

Taubman D S. 2008. Kakadu V6.0 Software. http://www.kakadusoftware.com

Tourapis A M, Leontaris A, Sühring K and Sullivan G. 2007. H.264/MPEG-4 AVC Reference Software Manual. JVT-X072, Ed. Geneva, CH

Wang Z, Bovik A C, Sheikh H R and Simoncelli E P. 2004. Image quality assessment: from error visibility to structural similarity. *IEEE Transactions on Image Processing*, **13**(4): 600—612

Wiegand T, Sullivan G J, Bjntegaard G and Luthra A. 2003. Overview of the H.264/AVC video coding standard. *IEEE Transactions on Circuits and Systems for Video Technology*, **13**(7): 560—576

Xia W P, Wang Z S and Han J Z. 2006. A real-time data compression algorithm for SAR complex images based on block adaptive quantization. *Journal of Image and Graphics*, **11**(8): 1097—1104

附中文参考文献

郭勐, 简方军, 张钦, 徐斌, 王贞松, 韩承德. 2007. 基于 FPGA 实现的星载 SAR 实时成像系统研究. 计算机研究与发展, **44**(3): 497—502

孙明, 李春升. 2006. 基于自适应加权方法的复值 SAR 图像的频域压缩改进算法. 电子与信息学报, **28**(1): 12—15

夏卫平, 王贞松, 韩冀中. 2006. 基于块自适应量化的 SAR 复数图像实时压缩算法. 中国图象图形学报, **11**(8): 1097—1104